HYDRODYNAMIC SLIP LENGTH OF WATER IN CARBON-BASED NANOCONFINEMENTS: A MOLECULAR DYNAMICS INVESTIGATION

Alper Tunga CELEBI[*], **Jafar GHORBANIAN**[**] **and Ali BESKOK**[***]

[*] Southern Methodist University, Lyle School of Engineering, 3101 Dyer Street Dallas, TX 75205, USA,
acelebi@smu.edu
[**] Southern Methodist University, Lyle School of Engineering, 3101 Dyer Street Dallas, TX 75205, USA,
jghorbanian@smu.edu
[***] Southern Methodist University, Lyle School of Engineering, 3101 Dyer Street Dallas, TX 75205, USA,
abeskok@smu.edu

Abstract: Molecular dynamics (MD) simulations of force-driven deionized water flows both in nanoscale periodic systems and in carbon-based nanoconfinements are performed. Carbon nanotubes (CNTs) and graphene nanochannels are considered to investigate the size and curvature effects on the slip length of water at a fixed thermodynamic state. Nanochannel flow simulations exhibit plug velocity profiles with large slip length at the interface that are modeled by Navier-type slip boundary condition. Large slip lengths are mainly due to the high surface density of carbon-based nanoconduits and weak interaction strengths between carbon atoms and water molecules. A constant slip length of 64 nm in graphene channels are observed for heights varying from 2.71 to 9.52 nm. However, considering comparable CNT diameters, slip lengths are found to be size-dependent. Slip length in CNTs decreases from 204 nm to approximately 68 nm with increased diameter.
Key Words: Nanochannel flows, molecular dynamics, slip length, graphene, carbon nanotube.

KARBON BAZLI NANOKANALLARDA SUYUN HİDRODİNAMİK KAYMA MESAFESİNİN MOLEKÜLER DİNAMİK YÖNTEMİ İLE İNCELENMESİ

Özet: Bu calışmada karbon-bazlı nanokanallar ve periyodik sistemlerdeki iyonsuz su akışları, moleküler dinamik simülasyonları ile incelenmiştir. Farklı boyutlara sahip karbon nanotüpler ve grafen kanalların içindeki kayma mesafeleri, sabit termodinamik koşullar altında elde edilmiştir. Kayma mesafesi Navier kayma sınır koşulları ile ifade edilip, kanal yüksekliğindeki hız profilleri kullanılarak hesaplanmıştır. Nanokanal simülasyonları boyut ve şekilden bağımsız olarak hem silindirik karbon nanotüplerde hem de düzlemsel grafen kanallarda sabit eksenel hız (plug) profilleri ve yüksek kayma mesafesi göstermiştir. Bu yüksek kayma mesafelerinin sebepleri, karbon nanokanalların sahip olduğu pürüzsüz yüzey alanı ve yüksek atom yoğunluğu ve bununla birlikte su molekülleri ile karbon atomları arasında oluşan zayıf moleküler arası bağlardır. Boyutları 2.71 nm ile 9.52 nm arasında değişen grafen kanalları için yaklaşık 64 nm büyüklüğünde sabit bir kayma mesafesi elde edilirken, bu parametrenin karbon nanotüplerde kanal çapının bir fonksiyonu olduğu tespit edilmiştir. Benzer boyutlara sahip karbon nanotüplerde, kayma mesafesi artan nanotüp çapı ile azalmakta olduğu gozlenmiştir, 204 nm ile 68 nm arası değişen kayma mesafeseleri elde edilmiştir.
Anahtar Kelimeler: Nanokanallarda akış, moleküler dinamik, kayma mesafesi, grafen, karbon nanotüp.

INTRODUCTION

Interest in nanoscale liquid transport has been increasing due to the potential use of nanochannels and nanotubes in many applications such as chemical detection (Eijkel & Van Den Berg, 2005), drug delivery (Angelova et al., 2008), nanofiltration (Cohen-Tanugi & Grossman, 2012) and biosensing (Karnik et al., 2006). In nanoscale confinements, surface area to volume ratio is very high, and the transport is dominated by the surface forces. For such scale systems, surface roughness and surface-liquid intermolecular interactions play a critical role to characterize the flow. In addition, scale reductions can lead to conditions where conduit dimensions are comparable to the molecular diameter, and a discrete motion of molecules can be observed. As a result, transport properties in nanoscale confinements may be substantially different than their macroscopic counterparts (Ghorbanian & Beskok, 2016).

Dominant interfacial effects are important in characterization of liquid flows in nanochannels (Karniadakis et al., 2006). Depending on the liquid-solid coupling at interface, liquids in nanosized channels can exhibit no-slip, stick or slip boundary conditions (Ghorbanian & Beskok, 2016). When the interaction strength between wall and liquid atoms is weaker than that of between liquid atoms, liquid atoms recede from

walls and a finite velocity-slip at interface is induced. This slip behavior is typically quantified by the concept of slip length, which is defined as the extrapolated distance relative to the wall where the tangential velocity becomes zero. The slip length has an essential role to assess the deviations from continuum flow theory at nanoscale. For pressure-driven flows in nanochannels, strong slip behavior indicates an enhanced liquid (water) flow, enabling flow-rates greater than the predictions of continuum-based no-slip Hagen-Poiseuille's relation (Holt et al., 2006; Majumder et al., 2005). Therefore, it is theoretically possible to establish super-fast water transport in nanoscale systems by choosing hydrophobic channels. For this purpose, carbon-based nanostructures such as carbon nanotube (CNT) and graphene are exceptional materials exhibiting a large slip behavior due to combined effect of their high atomic density, smooth surface and weak liquid-solid interaction strength (Joshi et al., 2014; Liu et al., 2015). Numerous computational and experimental studies focused on the determination of slip length of water in different sized carbon-based nanochannels. Multiple molecular dynamics (MD) simulations predicted the slip length of water in graphene nanochannels in a range of 30 to 80 nm (Falk et al., 2010; Koumoutsakos et al., 2003; Kannam et al., 2012; Ramos-Alvarado et al., 2016; Sam et al., 2018; J. A. Thomas & A. J. McGaughey, 2008; Xiong et al., 2011). Latest experiments conducted with graphene nanochannels indicated that slip lengths are scattered in the range of 1-200 nm for various channel heights, where it shows a statistical median of 16 nm (Xie et al., 2018). In addition, slip length in CNTs exhibit fundamental differences than that of graphene nanoconfinements due to the prominent curvature effect (Falk et al., 2010). Earlier pressure-driven water flow experiments (Qin, Yuan, Zhao, Xie, & Liu, 2011) and MD simulations (J. A. Thomas & A. J. McGaughey, 2008) showed that the slip length in CNT decreases with the increased tube diameter. Such studies indicated that the extent of slip length can be in the range of nanometers to a couple of micrometers as a function of CNT diameter.

Different methods are available in the literature for calculating the slip length in nanoconfinements using either equilibrium or non-equilibrium MD simulations. The former commonly employs Green-Kubo relation to determine friction coefficient, where the ratio of the friction coefficient to shear viscosity defines the slip length (Bocquet & Barrat, 1994; Kannam, Todd, Hansen, & Daivis, 2011). The latter considers external perturbation to the simulation domain for obtaining liquid flows. Non-equilibrium MD simulations provides a high accuracy, good statistics and low noise, ease of implementation at a moderate convergence time. For such simulations, the slip length can be evaluated by curve fitting to the MD predicted velocity profiles of force driven liquid flows (Celebi et al., 2017; Koumoutsakos et al., 2003; Kannam et al., 2012). For water flow in carbon-based nanochannels, velocity profiles show a plug-like behavior with a large velocity slip at the surface. This makes slip length very sensitive to the polynomial curve fitting and it can lead to large statistical errors (Kannam et al., 2012). Therefore, this study distinguishes itself by providing an alternate approach based on the integral form of conservation of linear momentum in the flow direction to estimate the slip length for plug like velocity profiles of CNTs and graphene nanochannels.

Although substantial progress has been made in determination of the slip length in carbon nanochannels, a consensus on its value as a function of channel size has not been reached yet. Most studies investigate the slip behavior of water either in CNTs or graphene nanochannels employing different methods. In addition, these studies differ in terms of intrinsic algorithmic details such as used water model in the simulations. Therefore, it is difficult to make a concrete comparison of slip in CNTs and graphene nanochannels for different sizes using literature data. This study presents a proper characterization of the slip length for both CNT and graphene nanochannels using a robust calculation method and provides a meticulous assessment of its size-dependence. The main objectives are to systematically examine the nanoconfinement effects in liquid slip flows and to assess the limitations of the continuum behavior. We first employ periodic domain simulations in absence of explicit walls to find the viscosity of adopted water model at the desired thermodynamic state. Then, MD simulations of force-driven water flows in planar graphene nanochannels and CNTs are performed for different channel sizes, and variations in density distributions, velocity profiles and slip lengths are presented. We provide an extended comparison of our results with previous MD studies in the literature and discussed the discrepancies. This paper is organized as follows. First, analytical description on calculation of the slip length in planar or cylindrical carbon nanochannels are explained. This is followed by the MD simulation details and results. In the end, our paper is finalized by giving the major conclusions.

THEORETICAL BACKGROUND

Liquid transport in nanochannels can be driven using external means such as pressure (Thomas, McGaughey, & Kuter-Arnebeck, 2010), electric fields (Celebi & Beskok, 2018), concentration gradients (Cracknell et al., 1995) and temperature (Shiomi & Maruyama, 2009) (Akkus et al., 2019). We consider force-driven water flow through uncharged graphene nanochannels and CNTs as illustrated in Figure 1. The momentum equation in the stream-wise direction for a steady, incompressible, fully developed, force-driven channel flow between reduces to

$$\frac{d^2u}{d\eta^2} = -\frac{f}{\mu} \qquad (1)$$

where $u(\eta)$, μ and f are the stream-wise velocity field, apparent viscosity of the liquid and the applied body force in the stream-wise (z) direction, respectively. It should be noted that 'η' is equal to 'y' in cartesian

coordinates while it is 'r' in cylindrical coordinate systems. Furthermore, Navier-type slip condition is utilized at the liquid-solid interface as

$$u_l - u_w = \beta \frac{du}{d\eta} \qquad (2)$$

where β, u_l and u_w are the slip length, liquid and wall velocities, respectively. Considering a constant slip length on both walls and the symmetry conditions at the channel center, the velocity profile of an incompressible Newtonian liquid between two parallel plates with a channel height of h is given by

$$u(y) = \frac{fh^2}{2\mu}\left(-\left(\frac{y}{h}\right)^2 + \left(\frac{y}{h}\right)\right) + \frac{fh\beta}{2\mu} \qquad (3)$$

For nanotubes, the velocity profile of an incompressible flow through a cylindrical tube with a radius R is given by

$$u(r) = \frac{fR^2}{4\mu}\left(-\left(\frac{r}{R}\right)^2 + 1\right) + \frac{fR\beta}{2\mu} \qquad (4)$$
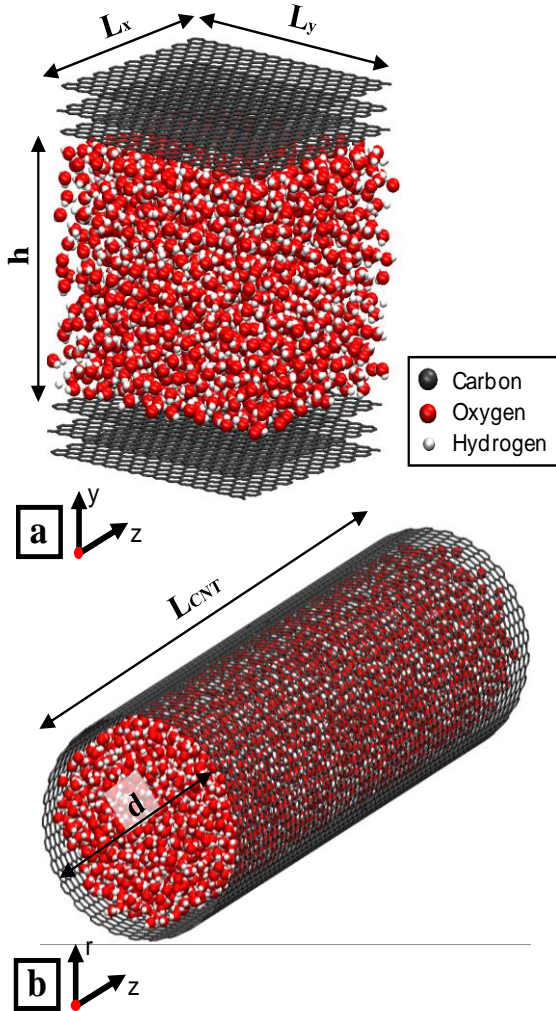
Figure 1. Schematic of the simulation domains (a) Planar graphene nanochannel and (b) CNT.

In Equations (3) and (4), the first term of the right-hand side is related to the parabolic profile of the typical no-slip solution (Ghorbanian & Beskok, 2016). The last term is related to flow enhancement due to slip, which is used to obtain the slip length for parabolic velocity profiles. The slip length normalized by the channel height ($\beta^* = \beta/h$) or CNT radius ($\beta^* = \beta/R$) are crucial on the shape of the velocity profile. The focal length (distance between the vertex and the focus) of the parabolic curve increases with increased β^*, and develops gradually flattened and ultimately "plug-like" velocity profiles. Using conservation of linear momentum in the flow direction, wall shear (τ_w) is balanced with the body force on water molecules (Celebi et al., 2018; Ghorbanian et al., 2016). Then, we combine this relation with the Navier-type slip condition in Equation (2) and the constitutive equation of shear stress for Newtonian fluids ($\tau_w = \mu \frac{du}{d\eta}$) to obtain the following relations for slip length

$$\beta = \begin{cases} \dfrac{2\mu u_s}{fh} \approx \dfrac{2\mu\bar{u}}{fh}, & \text{paralel plates} \\[2mm] \dfrac{2\mu u_s}{fR} \approx \dfrac{2\mu\bar{u}}{fR}, & \text{nanotubes} \end{cases} \qquad (5)$$

where u_s is the slip velocity and $\bar{u}$ is the channel averaged velocity. It is important to indicate that the slip velocity is practically equal to the average velocity for plug-like flows (Falk et al., 2010). In addition, bulk viscosity of the liquid (μ) is also crucial for defining the slip length.

SIMULATION DETAILS

Nonequilibrium MD simulations were performed using LAMMPS (Large Scale Atomic/Molecular Massively Parallel Simulator) (Plimpton, 1995). Lennard-Jones (LJ) potential was used to model van der Waals forces between the atoms, while Coulomb potential was used for electrostatic interactions of charged sites, given by

$$\emptyset(r_{ij}) = 4\varepsilon\left[\left(\frac{\sigma_{ij}}{r_{ij}}\right)^{12} - \left(\frac{\sigma_{ij}}{r_{ij}}\right)^6\right] \qquad (6)$$
$$+ \frac{1}{4\pi\epsilon_0}\sum_i^a\sum_j^b\frac{q_i q_j}{r_{ij}}$$

where ε and σ_{ij} are the well-depth and molecular distance, respectively. ϵ_0 is the vacuum permittivity, q_i and q_j are the atomic charges, r_{ij} is the distance between atoms or charged particles. Water interactions were described using rigid, four-site TIP4P/2005 model due to its good predictions of bulk viscosity of water (Abascal & Vega, 2005; Backer et al., 2005). Angles and bond length were constrained using SHAKE algorithm (Miyamoto & Kollman, 1992). Only oxygen atoms contributions were accounted in LJ calculations due to hydrogen's small size and mass (Wang et al., 2011). Interactions between carbon atoms and liquid molecules

were described based on experimental contact angle study (Werder et al., 2003). Carbon walls were fixed at their original positions and their interactions were excluded to maintain a cold wall behavior. Cold wall approach reduces the computational time, while it does not significantly alter the results (Celebi et al, 2014). No charges were assigned on the carbon atoms to represent an electrically neutral wall, but hydrogens and oxygens in water molecules carry partial charges. The long-range electrostatic interactions of charged particles were computed using the particle-particle-particle-mesh (PPPM) algorithm with a root-mean-accuracy of 10^{-5} (Plimpton, et al., 1997). The specified accuracy describes the relative root-mean-square error in per-atom force that is explicitly computed by the long-range algorithm. The reference value is selected as a representative of the magnitude of electrostatic forces in the simulation domain, where accuracy value of 10^{-5} indicates that the reference force is 100,000 greater than the root-mean-square error (Plimpton, 1995). Short-range interactions were smoothly truncated with a 1 nm cut-off distance. Table 1 presents potential parameters used for all atomic species.

Table 1. Potential parameters for atomic species.

Atom Pair	σ (nm)	ε (kj/mol)	q (e)
H – H	0	0	0.5564
O - O	0.31589	0.7749	-1.1128
C - O	0.3190	0.3921	0

In this study, each simulation begins with a thermal equilibrium using Canonical (NVT) ensemble before applying any external driving-forces on the liquid domain. To establish this, initial velocities of each water molecule were randomly assigned using Gaussian distribution at a specified temperature. The thermodynamic state was fixed by maintaining the temperature of water at 300 K using Nose-Hoover thermostat and keeping the bulk density of water at 997 kg/m^3. The systems were run for 2 ns to reach an equilibrium state. Starting from the equilibrium conditions, force-driven water flow simulations were carried out. The flow was driven by externally applied force on each water molecule in the stream-wise direction. All simulations are run with 1 fs time steps using Verlet integration scheme. Periodic boundary conditions were used in the flow direction. The time scale to reach steady solution was determined using time for momentum diffusion ($t_D = l^2/v$), where v is the kinematic viscosity and l is either the channel height or CNT radius. Steady state response was achieved by initially running the system for 1 ns, then an additional 16 ns was performed for data collection and statistical averaging. This creates 1600 independent time-averaged data sets. To calculate the standard deviation of slip lengths, we used 20 independent samples obtained from the averaging of 80 consecutive data sets. Planar and cylindrical binning were applied using 1000 slab-bins to properly resolve the wall-liquid interface for graphene

and CNT nanochannels, respectively. The bin size was determined so that density profiles don't exhibit significant variations, where it is fine enough to resolve the details at the interface.

RESULTS

Force-driven Water Flow Simulations in Periodic Domains

Fluid viscosity is critical for accurate characterization of slip in nanoscale confinements. Many interatomic potentials have been introduced for simulations of water, differing in the interaction parameters, the number of charged sites, their flexibility / rigidity and polarizability. Considering the classical water models, TIP4P/2005 was able to reproduce bulk properties of water in a wide range of temperatures (Fanourgakis, Medina, & Prosmiti, 2012; González & Abascal, 2010; Tazi et al., 2012). Initially, we perform counter-flowing periodic domain simulations in absence of explicit boundaries as explained in Backer et al. (Backer et al., 2005) to validate the viscosity of TIP4P/2005 water. First, periodic box is spatially divided into two identical subdomains and equal body forces are applied on each subdomain in opposing directions. This creates two counter flowing parabolic velocity profiles at each periodic side with zero velocity (i.e., no-slip) at the domain center. Figure 2 shows the obtained velocity profiles for two counter flows in a system size of 2h=9.52 nm. The velocity profiles on each subdomain are fitted to a second-order polynomial equation in the form of $u(z) = Ay^2 + By + C$. Then, the viscosity is found by comparing the coefficients of the fitted equations (parameters A and B) with the continuum flow model given by Equation (3) assuming no-slip conditions ($\beta = 0$). We calculate four different viscosity values following the methodology in Ghorbanian and Beskok (Ghorbanian & Beskok, 2016). Viscosities of μ_1 and μ_2 are calculated using the coefficients of A for each side of the curve fit by $\mu = -f/2A$, while μ_3 and μ_4 are calculated using the coefficients of B for each side of the curve fit by $\mu = -fh/2B$. Finally, their average value is used for comparison with the thermodynamic viscosity of water which is μ_{TD}=853 µPa.s at given thermodynamic conditions of T=300 K and ρ=997 kg/m^3.

In Table 2, the viscosity results of counter-flowing force-driven periodic water domain simulations are presented as a function of the domain size. Comparison of the thermodynamic viscosity value and MD-predicted average water viscosity shows a maximum error of 4.4% in the smallest domain size. The viscosity values are also in good agreement with the MD-predicted values reported for TIP4P/2005 water model in literature (Guevara-Carrion, Vrabec, & Hasse, 2011; Tazi et al., 2012). Clearly, periodic box simulation results assure the reliability of adopted water model in terms of apparent viscosity in periodic domains as small as 1.7 nm.

Table 2 indicates the viscosity of water without any explicit walls. However, in this study, we are interested

in viscosity of water model in nanoscale confinements. Multiple reports showed that bulk properties of liquids in nanoscale confinements are still observable for channel heights up to 2.5 nm (Markesteijn, Hartkamp, Luding, & Westerweel, 2012; Qiao & Aluru, 2003; Suk & Aluru, 2013; Travis, Todd, & Evans, 1997). For narrower channels (size smaller than 6-7 molecular diameters), confinement effect becomes very important, where liquid viscosity predicted by MD simulations is significantly larger than the bulk value (Bitsanis, Somers, Davis, & Tirrell, 1990). One main reason is that the wall effect results in density layering of liquid molecules near the walls. For small channels (sub 2.5 nm), density layering from both sides of the channel overlaps, which affects overall bulk properties of liquid. At sufficiently large channel heights, this density layering subsides and reaches a constant bulk density at the channel center. Aluru and Suk demonstrated that apparent viscosity of water in CNTs is larger at very small CNT diameters, then viscosity approaches to its bulk value with diameters above 2.5 nm (Suk & Aluru, 2013). Furthermore, using TIP4P/2005 water model, Markesteijn *et al.* carried out

Poiseuille flow simulations of 4.3 nm height planar nanochannel, and showed that viscosity of TIP4P/2005 water model correctly captures the thermodynamic value for a wide range of temperatures for this length scale (Markesteijn et al., 2012). In this study we consider channel heights larger than 2.5 nm except for the smallest case. Therefore, we use viscosity of TIP4P/2005 model in the slip calculation given in Equation (5), where it was proven as nearly equal to the thermodynamic value at 300K by periodic domain simulations

Force-driven Water Flow Simulations in Nanochannels

Next, force-driven water flow simulations are performed in graphene channels and CNTs at different sizes. The height of the graphene nanochannels are in the range of 1.94 to 9.52 nm, while CNTs have similar diameter between 1.90 to 9.49 nm. Due to their different sizes, the numbers of water molecules used for each simulation case are different. Figure 3(a) presents the density profiles of
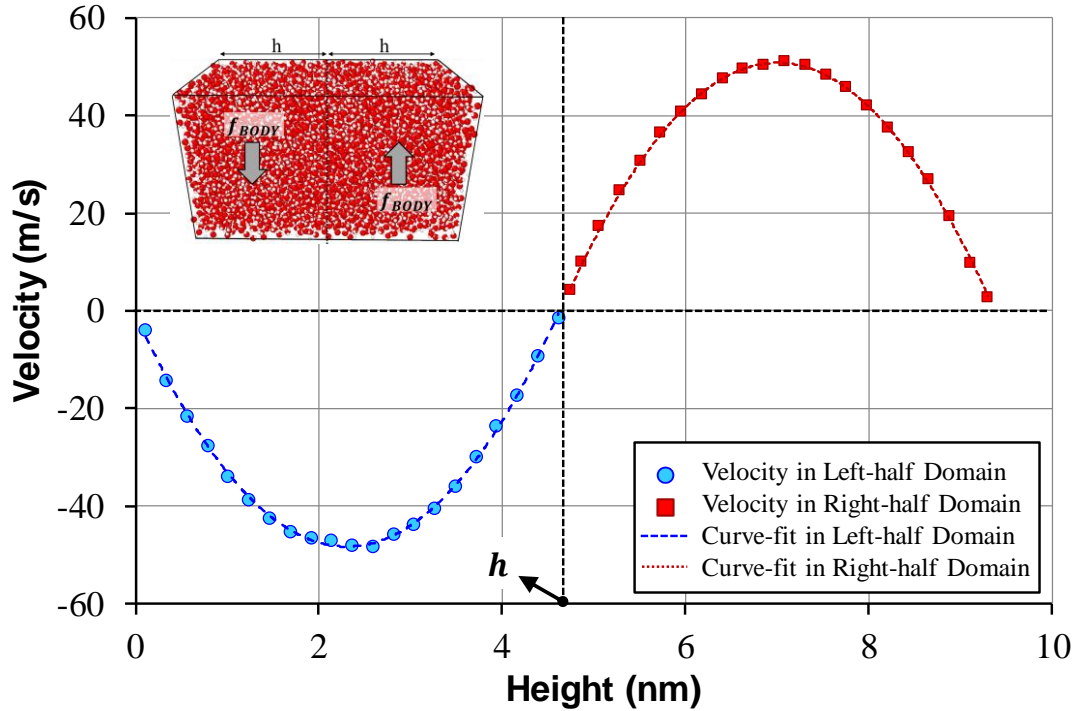
Figure 2. Force-driven counter-flowing of water in a periodic box of 2h=9.52 nm

Table 2. Viscosity results using polynomial curve-fitting method. Thermodynamic viscosity of water is 853 µPa.s at T=300 K and ρ=997 kg/m³

h (nm)	μ_1(µPa.s)	μ_2(µPa.s)	μ_3(µPa.s)	μ_4(µPa.s)	μ_{AVE}(µPa.s)	Error (%)
1.70	819.7	823.9	809.5	811.8	816.2	4.4
2.72	833.9	830.8	826.2	825.9	828.2	2.7
4.76	838.6	839.4	824.3	821.1	830.2	2.7
6.80	844.1	842.8	836.5	835.8	838.9	1.5
9.52	842.6	842.1	833.3	832.0	837.5	1.8

water in graphene nanochannels. Density distributions show a bulk region near the center of the channel and a layering region near the walls due to the wall force-field effect (Koplik & Banavar, 1995). At a fixed thermodynamic state, average density of liquid in nanoscale confinement is always lower than the desired thermodynamic value. This is because the average density within the layering region is lower than the bulk value (Ghorbanian et al., 2016). It is also known that the average density increases with increasing the channel height. In sufficiently large channels, the effect of density layering becomes very small and average density reaches the density at specified thermodynamic state. We found that liquid density layering in graphene nanoconfinements is still effective for channel heights up to 70 nm (Ghorbanian & Beskok, 2016). Above this length scale, the channel averaged density converges to

its thermodynamic value. Such results are also in good agreement with previous reports (Ghorbanian & Beskok, 2016; Wang & Hadjiconstantinou, 2015). As shown in Figure 3(a), water density in carbon confinements presents three distinct density peaks in all cases and the prominent first peak is located approximately 0.32 nm away from the solid walls. The distance between wall and first density peaks are similar at the lower and upper wall since it is mainly controlled by the constant Van der Waals parameters between carbon and oxygen atoms (Celebi et al., 2017; Ho & Striolo, 2013). This observation is important for fixing the thermodynamic state of water confined in narrow channels, where the density fluctuations from the two side walls overlap and the bulk region is lost. For such cases, Ghorbanian and Beskok
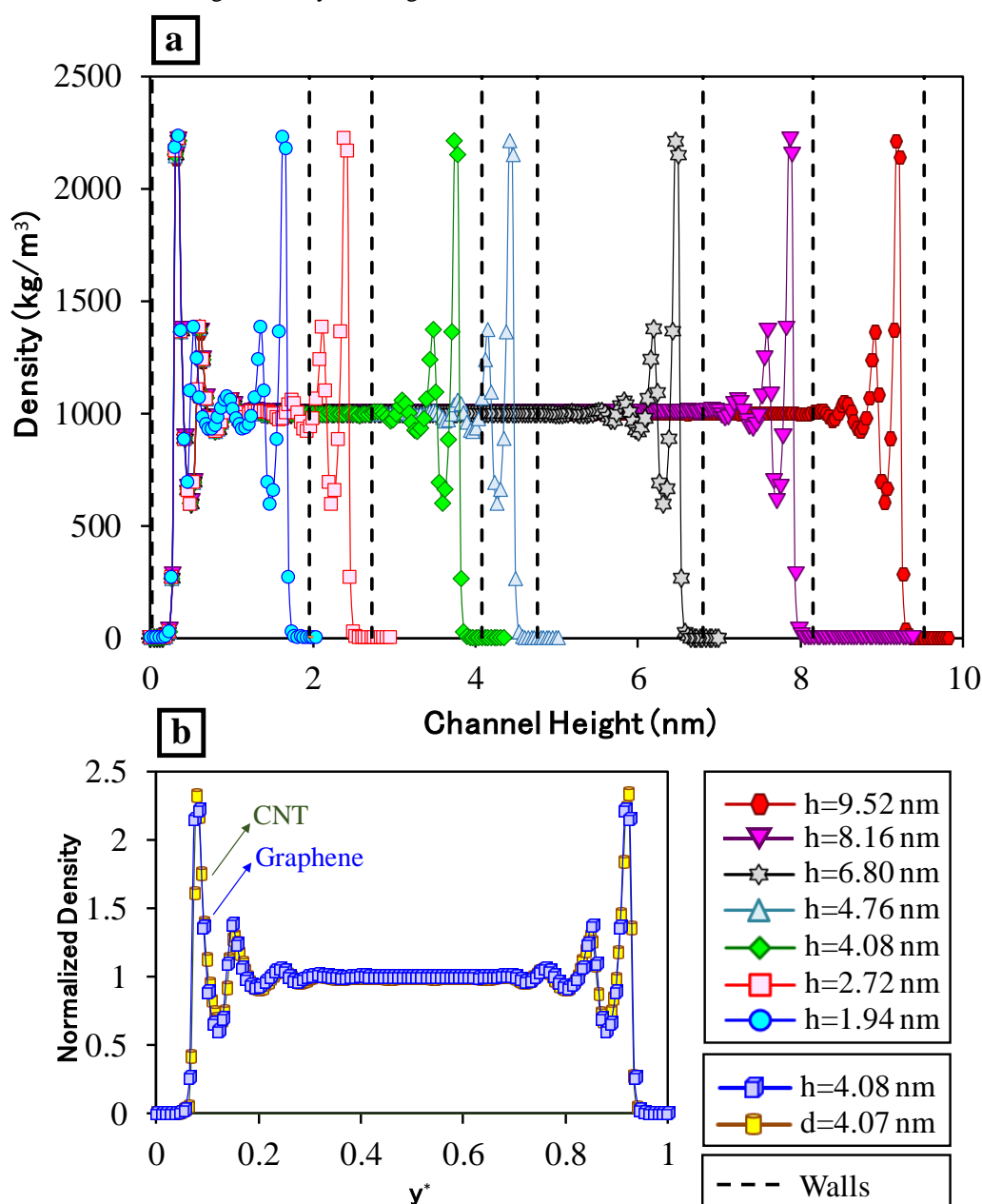
Figure 3. (a) Water density profiles in graphene nanochannels as a function of the channel height and (b) Comparison of normalized density profiles of water in CNT and Graphene nanoconfinements at similar sizes.
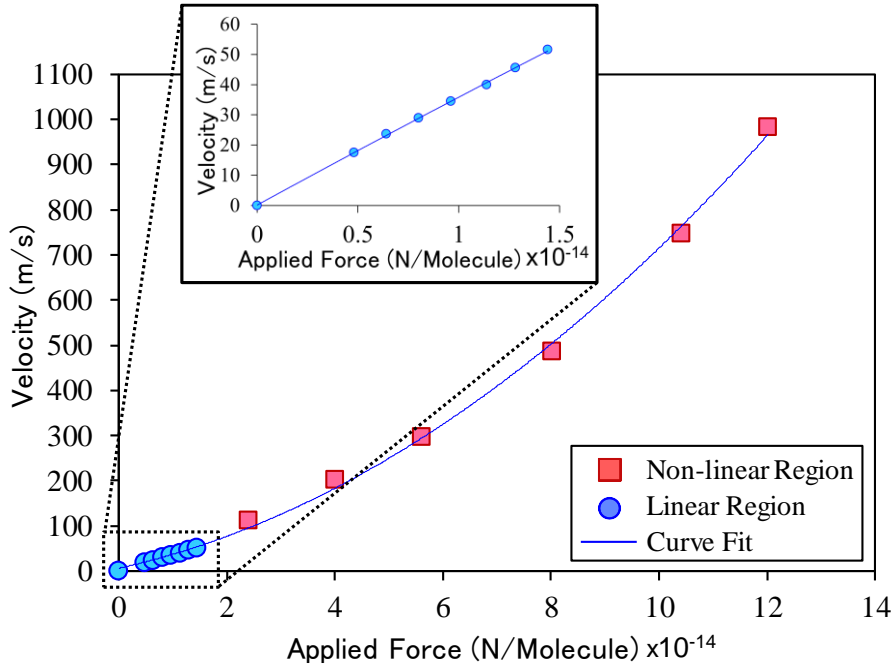
Figure 4. Average water velocity in graphene channels of 4.76 nm height as a function of the applied driving force.

equilibrated the nanochannel in a larger simulation domain and calculated the number of water molecules in the channel at the desired thermodynamic state (Ghorbanian & Beskok, 2016). Following their approach, we calculated the number of water molecules to be used in nanochannels smaller than 2.5 nm where density overlap happens and used these to maintain the thermodynamic state of water in simulations. In Figure 3(b), density profiles of water in CNT and graphene channels for similar pore sizes are compared. The density is normalized by average channel density ($\rho^* = \rho/\rho_{ave}$) while the y-axis is normalized by the channel height (y^* y/h) or CNT diameter ($y^* = y/d$), respectively. It can be seen that the locations and magnitudes of the density peaks for both geometries are very similar. We also utilize water density profiles to define effective channel dimensions and the location of the slip plane. It is well-known fact that liquid atoms cannot come close to the solid walls more than a molecular radius (Ghorbanian, 2017). This results in a finite gap (approximately one molecular diameter) between the first water density peak and the wall center locations as shown in Figure 3. The location of the first density peak is crucial because most of the water molecules are concentrated here due to the prescribed wall force-field and develop an apparent fluid region, whereas a discrete motion can be observed below this point. Addressing this, we can introduce the concept of an *effective channel height* as $h_e = h - 2L_0$, where L_O is the distance between the wall and the first density peak (Ghorbanian et al., 2016). For the case of CNT, one can define an *effective channel diameter* as $D_e = D - 2L_0$.

Liquid flows in nanochannels are induced by applying external forces on water molecules. Applied forces are chosen to ensure a linear response between the applied force and the resulting flow rate (Binder, Horbach, Kob, Paul, & Varnik, 2004; Sofos, Karakasidis, & Liakopoulos, 2009). It is important to avoid non-linear effects in computations, because it may ultimately result in unphysical or inaccurate transport properties including the slip length. Kannam et al. showed that slip length of an LJ liquid in graphene nanochannels diverges at increased external force fields (or shear rates for Couette flow) while it is constant at lower fields (Kannam et al., 2011). To establish the linear response regime, we systematically increase the total force and examine the channel averaged velocities. Figure 4 shows variations in the average water velocity in graphene nanochannel (for channel height of 4.76 nm) as a function of the applied force per water molecule. Clearly, nonlinear variations in the flow rate begin when the average channel velocities become larger than 50 m/s. Furthermore, the minimum flow velocities are selected as 25 m/s to reduce thermal noise, where better statistics are obtained.

In Figure 5(a), we present the velocity profiles of water in graphene nanochannels normalized by their average channel velocities at various size. Independent from the channel heights, all velocity profiles show plug-like flow behavior with large slip velocity at the liquid-solid interface. This is mostly due to frictionless nature of water flow on graphene surface. Weak interactions between wall atoms and water molecules result in non-wetted liquid system on carbon surfaces, implying large slip lengths (Voronov, Papavassiliou, & Lee, 2007). In addition, water velocity profiles in CNTs also present plug-flow behavior similar to the flow in graphene channels with large slip near the walls as shown in Figure 5(b). The plug velocity behavior implies that the average velocity difference is small from the channel center and

the wall, which allows us to use Equation (5) for slip length calculations. A maximum of 2.9% difference is observed between the channel average velocity and the channel center velocity. Kannam *et al.* extensively studied the weak parabolic component in velocity profiles and concluded that polynomial fitting leads to large errors in slip length calculations (Kumar Kannam et al., 2012). Furthermore, a substantial increase in the

driving force imposed stronger parabolic profiles due to the contribution of nonlinear effects (Kannam et al., 2011; Kumar Kannam et al., 2012)

In Table 3, we present the results of slip lengths as a function of channel height and CNT diameter. To evaluate the slip lengths of water in hydrophobic carbon nanochannels, we apply plug flow method
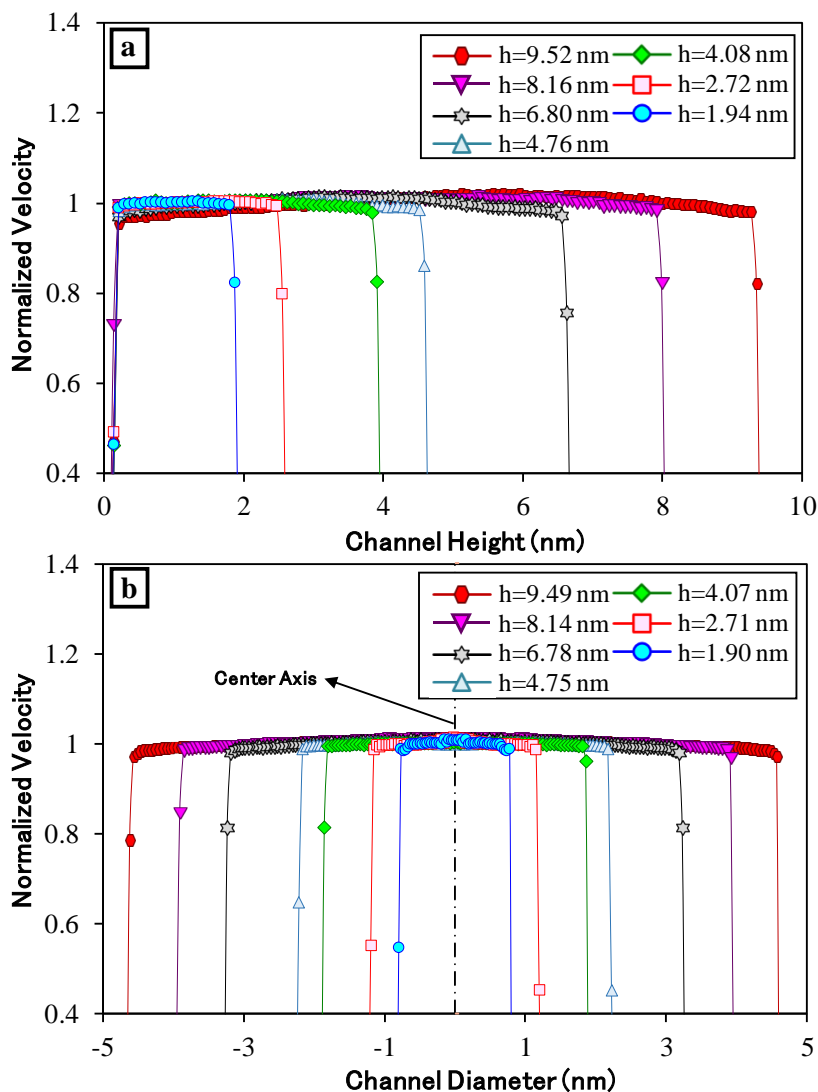
Figure 5. Water velocity profiles normalized by average channel velocities (a) as a function of height in graphene nanochannels (b) as a function of diameter in CNTs.

Table 3. Slip length values of water in graphene nanochannels and CNTs at various sizes.

Graphene Channels		Carbon Nanotubes	
h (nm)	β (nm)	d (nm)	β (nm)
9.52	64.2 ± 4.9	9.49	68.7 ± 5.5
8.16	63.8 ± 5.2	8.14	70.8 ± 6.0
6.80	63.0 ± 4.6	6.78	76.6 ± 6.2
4.76	63.1 ± 4.7	4.75	90.6 ± 8.6
4.08	64.1 ± 5.0	4.07	109.5 ± 9.5
2.72	65.8 ± 5.4	2.71	134.9 ± 11.8
1.94	76.4 ± 5.9	1.90	204.0 ± 16.3

given in Equation (5), which requires knowledge of apparent viscosity. We use thermodynamic viscosity of water (μ_{TD}=853 μPa.s) in this equation, since it is verified by the periodic box simulations as explained earlier. In addition, we use a slip plane located on the first water density peak (L_0) because the velocity profile within L_0 is not well defined due to low liquid density and rapidly reduces to zero. The slip lengths on the slip plane (β_{SP}) is related to that on the channel wall (β_W) by $\beta_{SP} = \beta_W + L_O$ (Celebi et al., 2017; Ghorbanian et al., 2016). The variations of the slip length values of water obtained in graphene nanochannels and CNTs as a function of channel size are represented in Figure 6(a) and Figure 6(b), respectively. Our MD results show that the slip-behavior is size-independent in graphene nanochannels for larger than 2 nm height. We predict the slip length of water in planar graphene channels approximately as 64 nm. This result is consistent with several slip length values previously reported in the literature (Kannam et al., 2011; Koumoutsakos et al., 2003; Kumar Kannam et al., 2012; Xiong et al., 2011). One can also notice that the slip length at the smallest channel height (1.94 nm) is found as 76 nm. For channels smaller than 2.5 nm height, definitions of local thermodynamic equilibrium and bulk liquid properties like density, and viscosity becomes inaccurate (Ghorbanian & Beskok, 2016; Qiao & Aluru, 2003; Travis et al., 1997). For such cases, the small number of liquid molecules inside the confinement is insufficient to represent a macroscopic hydrodynamic system, while the flow eventually shows a discrete liquid transport (Sam et al., 2018). Applicability of the continuum equations and constitutive laws can be challenged, and the calculation of the slip length and thermodynamic viscosity become irrelevant. Therefore, we illustrate the smallest channel sizes with hatched circle in Figure (6). Furthermore, velocity-slip of water in CNTs present a different behavior compared to that in graphene nanochannels. For such cases, curvature effect becomes substantial which changes the slip length as a function of the tube diameter (Falk et al., 2010). We show that slip length values vary between 204.0 nm and 68.7 nm for CNTs with diameters of 1.90 nm to 9.49 nm, respectively. Large slippage of water at the interface is induced at small diameters while it reduces with increased CNT size. This behavior is mainly related to the increased interfacial friction with increased CNT diameter. Small CNT diameters result in smoother surface potential energy landscape which creates smaller interfacial friction and large liquid slip at the surface (J. Thomas & A. McGaughey, 2008; J. A. Thomas & A. J. McGaughey, 2008). At sufficiently large CNT diameters, effects of surface curvature on the potential energy landscape becomes less sensitive to the increase in the channel size. Therefore, the size dependency of the slip becomes less prominent at larger CNT diameters. For instance, increasing CNT diameter from 8.14 nm to 9.49 nm decreases the slip length only from 70.8 nm to 68.7 nm. This trend is reasonable since the slip length is expected to converge slip length of water on a flat graphene as pointed out in earlier studies (J. Thomas & A. McGaughey, 2008; J. A. Thomas & A. J. McGaughey, 2008). In addition, the standard deviations for CNT diameter of 9.49 nm encapsulates the obtained slip length of water in flat graphene channels (64 nm). Moreover, we also estimate asymptotic values of slip length for larger scales by extrapolating the obtained slip data. After fitting MD-predicted slip lengths to a third-order polynomial equation, we find that slip length become equal to the that of graphene at CNT diameter of 12.1 nm. In Figure 6(b), we show this polynomial curve fitting with a dashed line (Note that the smallest channel size is not included in the fitting due to aforementioned reasons).

In Figure (6), slip length values of water in graphene and CNT channels in the present study are compared with multiple MD studies in the literature (Du et al., 2011; Falk et al., 2010; Huang et al.' 2008; Kannam et al., 2013; Kotsalis et al., 2004; Koumoutsakos et al., 2003; Kumar Kannam et al., 2012; Qin et al., 2011; Ramos-Alvarado et al., 2016; Sam et al., 2018; J. A. Thomas & A. J. McGaughey, 2008; Wagemann et al., 2017; Walther et al.,2013; Wei et al., 2014; Xiong et al., 2011). Although similar slip characteristics can be observed, there are also important quantitative differences on the slip lengths. These significant differences between MD studies are mainly due to the algorithmic details such as the use of different water models and interaction parameters, application of large body forces that result in nonlinear flow contributions, thermal/cold wall approximation and not properly fixing the thermodynamic state of the liquid. Furthermore, the slip length values based on experiments are much widely scattered. In earlier experiments, larger slip of water in CNTs were reported in the range of 1.4 μm to 54 μm for different tube diameters, where slip-modified continuum equations (See Equation (4)) were used to reproduce the measured flow rate (Holt et al., 2006; Majumder et al., 2005; Whitby & Quirke, 2007). In a recent study, slip lengths of water in CNTs were found between 300 nm to 15 nm for different tube diameters varying in the range of 15-50 nm, which follows the trend of slip reduction with increased diameter (Secchi et al., 2016). These results are much comparable with our MD simulations. For obtaining better insights and macroscopic comparisons with the experiment, Borg *et al.* recently proposed a multiscale computational approach based on coupled MD simulations and macroscopic flow resistance model to predict the water flow in various nanotube diameters (Borg et al., 2018). They employed Hagen-Poiseuille-Weissberg equation to show variations in viscosity, flow enhancement and slip length. The slip length of water in CNTs can be a couple of thousands of nanometers for CNTs with diameters smaller than 1.2 nm, while it is 61 nm on graphene. For graphene nanochannels, latest experiments by Xie *et al.* showed a scattered slip data varying between 0 to 200 nm at various channel heights without any distinct size dependence but follows a log normal distribution. Then, a median of the slip length as a single value of 16 nm after further statistical analysis (Xie et al., 2018). In another study, the slip length of water on graphite surface was measured as 8 nm. (Maali, Cohen-Bouhacina, & Kellay, 2008) Numerous factors in experiments such as measurement uncertainties, possible imperfections on the graphitic surface, impurities in water, static charges on the carbon surfaces and entrance/exit effects should be considered.
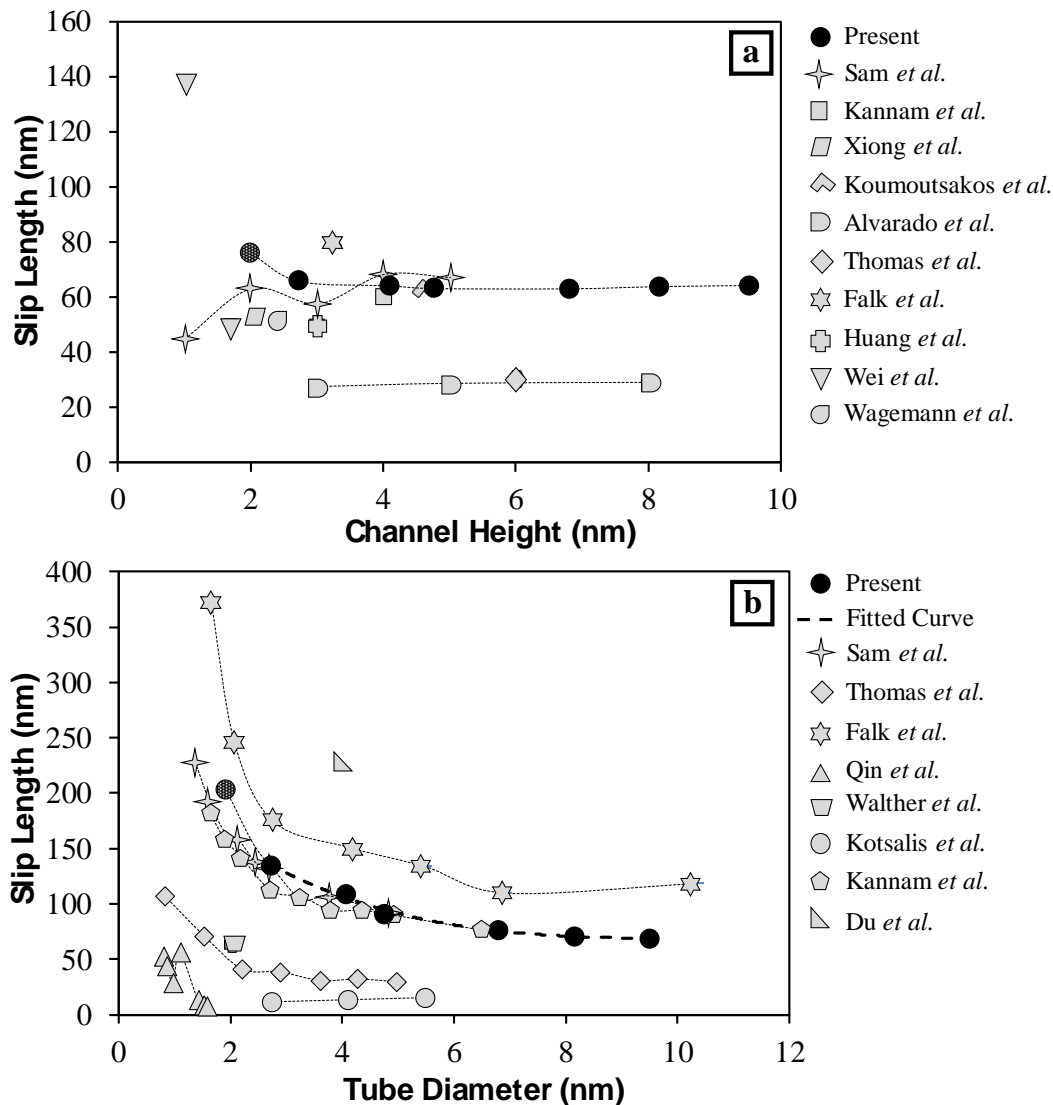
Figure 6. Slip length of water in (a) graphene nanochannels and (b) CNTs as a function of channel height and tube diameter. Our results (black circles) are compared with MD results in the literature.

CONCLUSION

Force-driven water flows through different sized graphene nanochannels and CNTs are investigated using MD simulations. Simulations are carried out for nanoconfinements heights in the range of 1.9 nm to 9.52 nm. Local thermodynamic equilibrium is maintained in nanochannel flows at a fixed thermodynamic state by keeping the bulk density constant at 997 kg/m^3 at 300 K using Nose-Hoover thermostat. Within the scopes of this work, the following conclusions could be drawn

- Force-driven periodic domain simulations ensure Newtonian behavior of water for domain sizes as small as 1.7 nm. The viscosity of water at the specified thermodynamic state is found with a maximum deviation of 4.4% from the thermodynamic bulk value

- Water density profiles are similar for both CNTs and graphene nanochannels at comparable sizes. In

addition, average density of water at a fixed thermodynamic state are lower than the thermodynamic value due to effect of density layering. This prominent effect is observable for channel heights up to 70 nm.

- Linear flow response regime is systematically investigated by increasing the applied body force. The non-linear responses begin to form for average velocities higher than 50 m/s.

- Independent from the channel-size and curvature, force-driven nanochannel flow simulations show plug-like velocity profiles with large slip lengths at interface.

- Slip length of water in graphene nanochannels shows size-independency for channel heights larger than 2 nm and it is approximately found as 64 nm. At smaller scales, classical continuum flow theories are not

146

applicable to describe the flow due to inaccurate local thermodynamic equilibrium and bulk liquid properties

- In CNTs, a curvature dependent slip behavior is observed. A slip length of 200 nm is found for the smallest CNT diameter (1.9 nm). Increased CNT diameters monotonically reduces the slip length until it converges to slip length on graphene.

REFERENCES

Abascal J.L. and Vega C., 2005, A general purpose model for the condensed phases of water, *J Chem Phys,* 123, 234505.

Angelova A., Angelov B., Lesieur S., Mutafchieva R., Ollivon M., Bourgaux C., Willumeit R. and Couvreur P, 2018, Dynamic control of nanofluidic channels in protein drug delivery vehicles, *J. Drug Deliv. Sci. Technol.* 18, 41-45.

Akkus Y., Nguyen C.T., Celebi A.T. and Beskok A., 2019, A first look at the performance of nano-grooved heat pipes, *Int. J. Heat Mass Transfer,* 132, 280-287.

Backer J., Lowe C., Hoefsloot H. and Iedema P, 2005, Poiseuille flow to measure the viscosity of particle model fluids, *J. Chem. Phys.*, 122, 154503.

Binder K., Horbach J., Kob W., Paul W. and Varnik F., 2004, Molecular dynamics simulations, *J. Phys.: Condens. Matter*, 16, S429.

Bitsanis I., Somers S.A., Davis H.T., Tirrell M., 1990, Microscopic dynamics of flow in molecularly narrow pores, *J. Chem. Phys.*, 93, 3427-3431.

Bocquet L. and Barrat J.-L., 1994, Hydrodynamic boundary conditions, correlation functions, and Kubo relations for confined fluids, *Phys. Rev. E,* 49, 3079.

Borg M.K., Lockerby D.A., Ritos K. and Reese J.M., 2018, Multiscale simulation of water flow through laboratory-scale nanotube membranes, *J. Membr. Sci.*, 567, 115-126.

Celebi A.T., Kirca M., Baykasoglu C., Mugan A., and To, A.C., 2014, Tensile behavior of heat welded CNT network structures, *Comput. Mater. Sci.*, 88, 14-21

Celebi A.T., Barisik M. and Beskok A., 2017, Electric field controlled transport of water in graphene nano-channels, *J. Chem. Phys.*, 147, 164311.

Celebi A.T., Barisik M. and Beskok A., 2018, Surface charge-dependent transport of water in graphene nano-channels, *Microfluid. Nanofluid.*, 22, 7

Celebi A.T. and Beskok A., 2018, Molecular and Continuum Transport Perspectives on Electroosmotic Slip Flows, *J. Phys. Chem. C*, 122, 9699-9709.

Cohen-Tanugi D. and Grossman J.C., 2012, Water desalination across nanoporous graphene, *Nano Lett.*, 12, 3602-3608.

Cracknell R.F., Nicholson D. and Quirke N., 1995, Direct molecular dynamics simulation of flow down a chemical potential gradient in a slit-shaped micropore, *Phys. Rev. Lett.*, 74, 2463.

Du F., Qu L., Xia Z., Feng L. and Dai L., 2011, Membranes of vertically aligned superlong carbon nanotubes, *Langmuir*, 27, 8437-8443.

Eijkel J.C. and Van Den Berg A., 2005, Nanofluidics: what is it and what can we expect from it?, *Microfluid. Nanofluid.*, 1, 249-267.

Falk K., Sedlmeier F., Joly L., Netz R.R. and Bocquet L., 2010, Molecular origin of fast water transport in carbon nanotube membranes: superlubricity versus curvature dependent friction, *Nano Lett.*, 10, 4067-4073.

Fanourgakis G.S., Medina J. and Prosmiti R., 2012, Determining the bulk viscosity of rigid water models, *J. Phys. Chem. A*, 116, 2564-2570.

Ghorbanian J. and Beskok A., 2016, Scale effects in nano-channel liquid flows, *Microfluid. Nanofluid.*, 20, 121.

Ghorbanian J., Celebi A.T. and Beskok A., 2016, A phenomenological continuum model for force-driven nano-channel liquid flows, *J. Chem. Phys.*, 145, 184109.

Ghorbanian J., 2017, Thermal-Fluid Transport Phenomena in Nano-Scale Liquid Flows, Southern Methodist University.

González M.A. and Abascal J.L., 2010, The shear viscosity of rigid water models, *J. Chem. Phys.*, 132, 096101.

Ho T.A. and Striolo A., 2013, Polarizability effects in molecular dynamics simulations of the graphene-water interface, *J. Chem. Phys.*, 138, 054117.

Holt J.K., Park H.G., Wang Y., Stadermann M., Artyukhin A.B., Grigoropoulos C.P., Noy A. and Bakajin O., 2006, Fast mass transport through sub-2-nanometer carbon nanotubes, *Science*, 312, 1034-1037.

Huang D.M., Cottin-Bizonne C., Ybert C. and Bocquet L., 2008, Aqueous electrolytes near hydrophobic surfaces: Dynamic effects of ion specificity and hydrodynamic slip, *Langmuir*, 24, 1442-1450.

Joshi R., Carbone P., Wang F-C., Kravets V.G., Su Y., Grigorieva I.V., Wu H., Geim A.K. and Nair R.R., 2014,

Precise and ultrafast molecular sieving through graphene oxide membranes, *Science*, 343, 752-754.

Kannam S.K., Todd B., Hansen J.S. and Daivis P.J., 2013, How fast does water flow in carbon nanotubes? *J. Chem. Phys.*, 138, 094701.

Kannam S.K., Todd B., Hansen J.S. and Daivis PJ, 2011, Slip flow in graphene nanochannels, *J. Chem. Phys.*, 135, 016313.

Karniadakis G.E., Beskok A. and Aluru N., 2006, *Microflows and nanoflows: fundamentals and simulation,* Springer Science & Business Media.

Karnik R., Castelino K. and Majumdar A., 2006, Field-effect control of protein transport in a nanofluidic transistor circuit, *Appl. Phys. Lett.*, 88, 123114.

Koplik J. and Banavar J.R., 1995, Continuum deductions from molecular hydrodynamics, *Annual Review of Fluid Mechanics*, 27, 257-292.

Kotsalis E., Walther J. and Koumoutsakos P., 2004, Multiphase water flow inside carbon nanotubes, *Int. J. Multiphase Flow*, 30, 995-1010.

Koumoutsakos P., Jaffe R., Werder T. and Walther J., 2003, On the validity of the no-slip condition in nanofluidics, Laudon M (ed) 2003 Nanotechnology Conference and Trade Show, vol 1. Computational Publications. San Francisco, California, USA, pp 148–151

Kumar Kannam S., Todd B., Hansen J.S. and Daivis P.J., 2012, Slip length of water on graphene: Limitations of non-equilibrium molecular dynamics simulations, *J. Chem. Phys.*, 136, 024705.

Liu G., Jin W. and Xu N., 2015, Graphene-based membranes, *Chem. Soc. Rev.*, 44, 5016-5030.

Maali A,. Cohen-Bouhacina T. and Kellay H., 2008, Measurement of the slip length of water flow on graphite surface. *Appl Phys Lett* 2008, 92:053101.

Majumder M., Chopra N., Andrews R. and Hinds B.J., 2005, Nanoscale hydrodynamics: enhanced flow in carbon nanotubes, *Nature*, 438, 44.

Markesteijn A., Hartkamp R., Luding S. and Westerweel J., 2012, A comparison of the value of viscosity for several water models using Poiseuille flow in a nano-channel, *J. Chem. Phys.*, 136, 134104.

Miyamoto S. and Kollman P.A., 1992, SETTLE: an analytical version of the SHAKE and RATTLE algorithm for rigid water models, *J. Comput. Chem.*, 13, 952-962.

Plimpton S., Pollock R. and Stevens M., 1997, Particle-Mesh Ewald and rRESPA for Parallel Molecular Dynamics Simulations. In: Proceedings of the eighth SIAM conference on parallel processing for scientifc computing, p 8e21.

Plimpton S., 1995, Fast parallel algorithms for short-range molecular dynamics, *J. Comput. Phys.*, 117, 1-19.

Qiao R. and Aluru N., 2003, Ion concentrations and velocity profiles in nanochannel electroosmotic flows, *J. Chem. Phys.*, 118, 4692-4701.

Qin X., Yuan Q., Zhao Y., Xie S. and Liu Z., 2011, Measurement of the rate of water translocation through carbon nanotubes, *Nano Lett.*, 11, 2173-2177.

Ramos-Alvarado B., Kumar S. and Peterson G., 2016, Hydrodynamic slip length as a surface property, *Phys. Rev. E*, 93, 023101.

Sam A., Hartkamp R., Kannam S.K. and Sathian S.P., 2018, Prediction of fluid slip in cylindrical nanopores using equilibrium molecular simulations, *Nanotechnology*, 29, 485404.

Secchi E., Marbach S., Niguès A., Stein D., Siria A. and Bocquet L., 2016, Massive radius-dependent flow slippage in carbon nanotubes, *Nature*, 537, 210.

Shiomi J. and Maruyama S., 2009, Water transport inside a single-walled carbon nanotube driven by a temperature gradient, *Nanotechnology*, 20, 055708.

Sofos F., Karakasidis T. and Liakopoulos A., 2009, Transport properties of liquid argon in krypton nanochannels: anisotropy and non-homogeneity introduced by the solid walls, *Int. J. Heat Mass Transfer*, 52, 735-743.

Suk M. and Aluru N., 2013, Molecular and continuum hydrodynamics in graphene nanopores, *RSC Advances*, 3, 9365-9372.

Tazi S., Boţan A., Salanne M., Marry V., Turq P. and Rotenberg B., 2012, Diffusion coefficient and shear viscosity of rigid water models, *J. Phys.: Condens. Matter*, 24, 284117.

Thomas J. and McGaughey A., 2008, Density, distribution, and orientation of water molecules inside and outside carbon nanotubes, *J. Chem. Phys.*, 128, 084715.

Thomas J.A., McGaughey A.J. and Kuter-Arnebeck O., 2010, Pressure-driven water flow through carbon nanotubes: Insights from molecular dynamics simulation, *Int. J. Therm. Sci.*, 49, 281-289.

Thomas J.A. and McGaughey A.J., 2008, Reassessing fast water transport through carbon nanotubes, *Nano Lett.*, 8, 2788-2793.

Travis K.P., Todd B. and Evans D.J., 1997, Departure from Navier-Stokes hydrodynamics in confined liquids, *Phys. Rev. E*, 55, 4288.

Voronov R.S., Papavassiliou D.V. and Lee L.L., 2007, Slip length and contact angle over hydrophobic surfaces, *Chem. Phys. Lett.*, 441, 273-276.

Wagemann E., Oyarzua E., Walther J.H. and Zambrano H.A., 2017, Slip divergence of water flow in graphene nanochannels: the role of chirality, *PCCP*, 19, 8646-8652.

Walther J.H., Ritos K., Cruz-Chu E.R., Megaridis C.M. and Koumoutsakos P., 2013, Barriers to superfast water transport in carbon nanotube membranes, *Nano Lett.*, 13, 1910-1914.

Wang G.J. and Hadjiconstantinou N.G., 2015, Why are fluid densities so low in carbon nanotubes?, *Phys. Fluids*, 27, 052006.

Wang Y., Wang Y., Chen K. and Li B., 2011, Non-Equilibrium Molecular Dynamics Simulation of Electrokinetic Effects on Heterogeneous Ionic Transport in Nano-Channel, *Chem. Eng. Sci.*, 66, 2807−2816.

Wei N., Peng X. and Xu Z., 2014, Understanding water permeation in graphene oxide membranes, *ACS applied materials & interfaces*, 6, 5877-5883.

Werder T., Walther J.H., Jaffe R., Halicioglu T. and Koumoutsakos P., 2003, On the water− carbon interaction for use in molecular dynamics simulations of graphite and carbon nanotubes, *J. Phys. Chem. B*, 107, 1345-1352.

Whitby M. and Quirke N., 2007: Fluid flow in carbon nanotubes and nanopipes. *Nature Nanotechnology*, 2, 87.

Xie Q., Alibakhshi M.A., Jiao S., Xu Z., Hempel M., Kong J., Park H.G. and Duan C., 2018, Fast water transport in graphene nanofluidic channels, *Nature nanotechnology,* 13, 238-245.

Xiong W., Liu J.Z., Ma M., Xu Z., Sheridan J. and Zheng Q., 2011, Strain engineering water transport in graphene nanochannels, *Phys. Rev. E*, 84, 056329.